Novel diode laser-based sensors for gas sensing applications

3 authors:

Frank K Tittel
Rice University

800 PUBLICATIONS **14,759** CITATIONS

SEE PROFILE

David Lancaster
University of South Australia

112 PUBLICATIONS **1,266** CITATIONS

SEE PROFILE

Dirk Richter
University of Colorado Boulder

110 PUBLICATIONS **1,938** CITATIONS

SEE PROFILE

Some of the authors of this publication are also working on these related projects:

Project Cornell Dissertation Work View project

Project Waveguide based Chip Lasers View project

Novel Diode Laser-Based Sensors for Gas Sensing Applications

F. K. Tittel, D. G. Lancaster, and D. Richter

Rice Quantum Institute, Rice University, MS 366, Houston, TX, 77005 USA

e-mail: fkt@rice.edu

Abstract—The development of compact spectroscopic gas sensors and their applications to environmental sensing will be described. These sensors employ mid-infrared difference-frequency generation (DFG) in periodically poled lithium niobate (PPLN) crystals pumped by two single-frequency solid state lasers such as diode lasers, diode-pumped solid state, and fiber lasers. Ultrasensitive, highly selective, and real-time measurements of several important atmospheric trace gases, including carbon monoxide, nitrous oxide, carbon dioxide, formaldehye, and methane, have been demonstrated.

1. INTRODUCTION

Difference-frequency mixing of near-infrared cw laser sources is a convenient technique to spectrally shift visible and infrared lasers into the mid-infrared spectral region. By utilizing the recent commercial availability of novel nonlinear optical materials such as periodically poled lithium niobate (PPLN), and frequency-stable, single-mode diode lasers in the 0.8- to 2-μm spectral region, the key optoelectronic components exist to generate microwatt level radiation in the 3- to 5-μm range [1]. This spectral region is significant, as many molecules have strong fundamental rotational–vibrational absorption lines, which permit sensitive and absolute concentration measurements. Our motivation is to develop a compact difference-frequency-based trace gas sensor that is widely tunable, rugged, and cost effective. The requirements for such a sensor include room temperature and real-time operation, narrow bandwidth to minimize spectral interference, adequate signal-to-noise for the available infrared detectors, a robust design (suitcase size), inherent frequency stability (with no mode hopping behavior), and wide wavelength tunability for multiple trace gas species detection.

In recent work, this group has reported trace gas sensors generating microwatt-level radiation based on difference-frequency mixing (DFM) (using discrete optical components positioned on a compact optical bench) of Fabry–Perot style diode lasers with a Nd : YAG laser [2] and a 1083-nm distributed Bragg reflector (DBR) diode laser [3]. The former system proved sufficiently robust to be used in a successful one-month field test involving high-sensitivity H_2CO detection [4]. Widely tunable sensors based on difference-frequency mixing of an extended cavity diode laser (ECDL) and a Nd : YAG laser have also been reported [5, 6] and are suitable for multicomponent trace gas monitoring. More recently a laboratory prototype DFM-based gas sensor that utilizes single-mode fiber delivery and rare earth doped fiber amplifiers producing up to 11 μW of tunable mid-infrared radiation was demonstrated [7, 8]. The use of fiber delivery and fiber beam combining in these systems eliminates most of the routine alignment and stability problems inherent in difference-frequency mixed sources using discrete optics. The work we report here is an optical sensor architecture that is widely tunable with virtually no realignment required and packaged for portable field operation. This sensor uses two-frequency stable pump diode lasers, namely an ECDL employing a high power, single-frequency InGaAs laser and a 1083-nm distributed Bragg reflector (DBR) diode laser. Several trace gas species can be accessed in the 3.25- to 4.4-μm operating range of this field-ready, fiber-based DFG sensor. The predicted and experimentally measured PPLN phase matching conditions were also determined.

2. EXPERIMENTAL CONFIGURATION

The DFM-based gas sensor as shown in Figs. 1 and 2 consists of a 25-mW ECDL that is continuously tunable from 814 to 870 nm (no mode hopping behavior is observed), and a 50-mW, 1083-nm distributed Bragg reflector diode laser (DBR). The output from the DBR diode laser is collimated using an aspheric lens, passes through a –45 dB optical isolator, and is then coupled to a 6.6-μm core diameter single longitudinal mode (SLM) fiber terminated with a FC–APC style connector (threaded connector with the tip polished at 8° from normal incidence). A power of 12 mW of the seed radiation from the DBR diode laser is launched into the fiber. To increase the mechanical rigidity of the coupling arrangement, no beam correction optics were
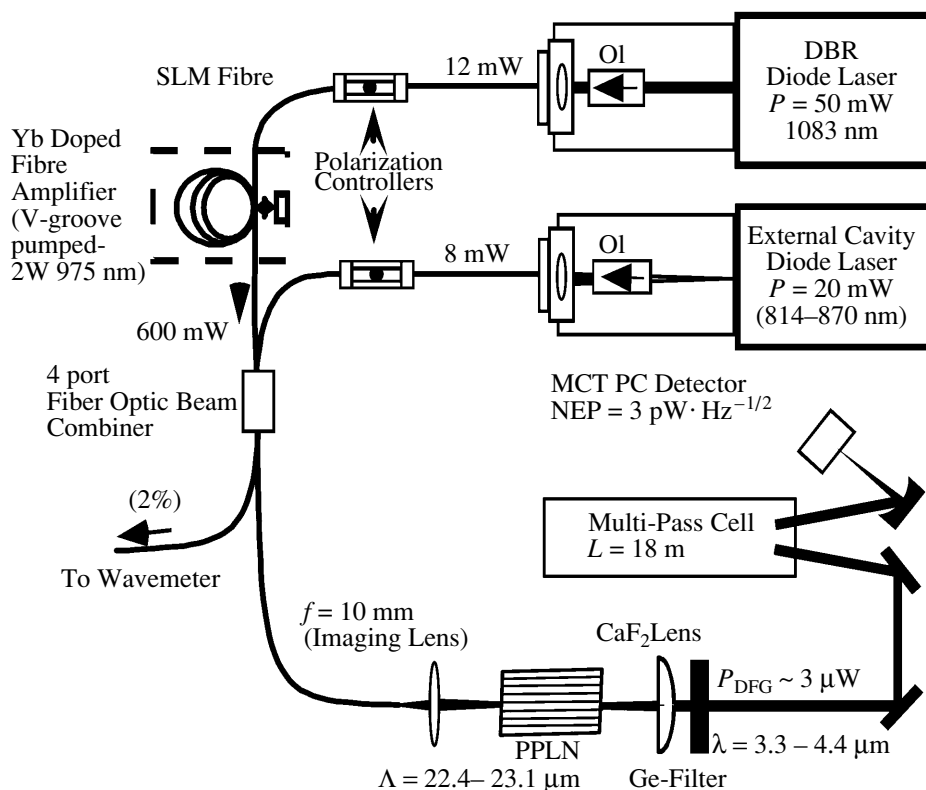
Fig. 1. Schematic diagram of the extended cavity diode laser and diode laser seeded 1083 nm Yb amplifier pumped difference frequency spectrometer.

used and the entire diode/optics assembly was mounted on a compact stainless steel miniature bench. Although higher coupling efficiencies into the fiber can be achieved, this was not necessary for this application, as only several mW of injected power at 1083 nm was required to saturate an Yb fiber amplifier [7, 8]. An amplifier output power of 590 mW at 1083 nm is obtained. This fiber was fusion spliced to the counter-propagating side (with respect to the 975-nm pump) of a 7.2-m ytterbium-doped fiber amplifier pumped by a 975-nm, 2-W diode laser. A V-groove geometry was used to launch the amplifier pump light into the Yb^{3+} doped double-cladding fiber [9, 10]. All amplifier components were packaged into a $9 \times 11 \times 2 \ cm^3$ housing.

The ECDL pump beam passed through a –30 dB optoisolator and was launched into a 5.5-µm core diameter SLM fiber using a single fiber-port assembly with a 48% optical coupling efficiency. Coarse frequency tuning of a Littman-type ECDL was achieved by "rotation" of its tuning mirror with respect to the diffraction grating. The advantage of the Littman ECDL configuration is the consistent beam-pointing stability as a function of wavelength over the entire ECDL tuning range, ensuring consistent coupling into the optical fiber. Fine tuning and approximately linear repetitive scanning (at <200 Hz) over single or multicomponent

absorption lines of up to ~25 GHz (0.83 cm^{-1}) was accomplished by linear current modulation of the DBR diode laser. Tuning the DBR diode laser was used in preference to the slower, nonlinear tuning available from the piezoelectrically modulated grating of the ECDL that tended to reduce its spectral stability.

The pump wavelengths were combined by a four-port fiber coupler (two in and two out), with losses of 9 and 8% at 1083 and 830 nm, respectively. An additional advantage of the fiber coupler is the availability of several percent of power at each wavelength at the second output fiber, thereby allowing the use of an on-line fiber-coupled wavemeter for frequency monitoring of the pump light. The linear polarization output from the launch fiber for an $e + e \longrightarrow e$ difference-frequency generation (DFG) process in the PPLN crystal was maintained by using two polarization controllers in the fiber delivery system. An achromat lens ($f = 10$ mm, 0.25 NA) was used for imaging the fiber output (terminated with an FC–APC connector) into the PPLN crystal. A 19-mm-long, 0.5-mm-thick PPLN crystal with a broadband AR-coating applied to both end faces contained 8 quasi-phasematching channels (0.5 mm wide) from 22.4–23.1 µm in 0.1-µm increments. To characterize the PPLN crystal phase matching, the crystal was mounted on a temperature-controlled copper block
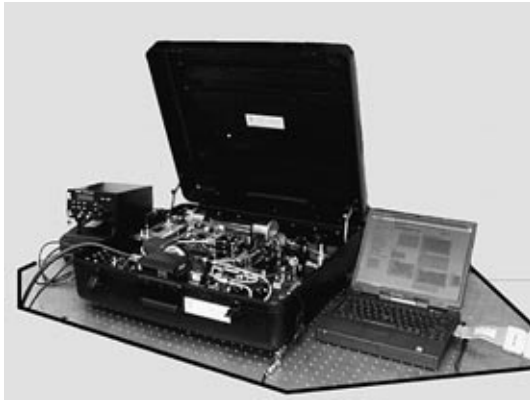
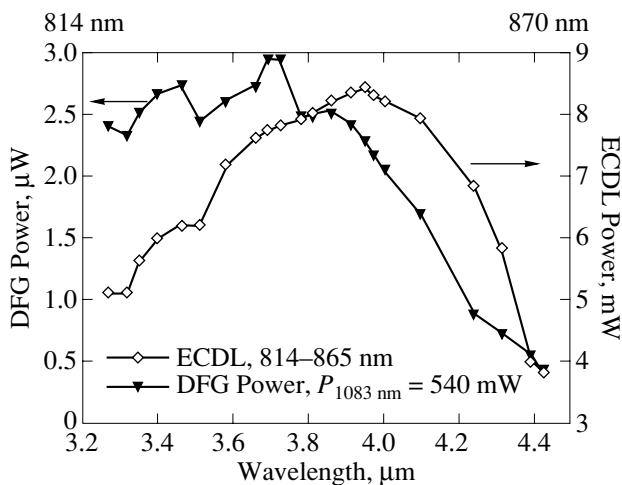**Fig. 2.** Photograph of DFG based gas sensor.

Fig. 3. DFG power as a function of idler wavelength and the ECDL power coupled into the optical fiber as a function of ECDL wavelength.

$(20 \times 15 \times 10 \text{ mm}^3)$ heated by a resistive element that allowed the crystal to be operated at higher temperatures ($<250°C$). The temperature at the copper block surface was measured by a cold-junction compensated thermocouple (2% accuracy). To reduce the thermal resistance between the copper block and crystal, thermal heat-sink compound was used. However, in the portable sensor configuration, the PPLN crystal was mounted on a single stage thermoelectric element, which could be operated at regulated temperatures ranging from 10 to 85°C. The lower temperature limit was set by concern for water condensation on the crystal faces.

The DFG radiation was collimated by a 5-cm focal length CaF_2 lens and the residual pump light was blocked by a 3-mm-thick AR-coated germanium filter. The radiation was either focused directly on the three-stage Peltier cooled HgCdTe (MCT) detector for power measurements or directed through an 18-m-pathlength

multipass spectroscopic cell (physically 30 cm long) and then focused onto the detector. In both cases the radiation was focused onto the detector by use of a 5-cm focal length gold coated off-axis parabolic mirror. The MCT detector, with a 1-mm^2 active area and a measured noise equivalent power of 3 pW/Hz$^{-1/2}$, was DC coupled to a low-noise preamplifier operating in a photoconductive mode.

In order to reduce the size of the driver electronics required for the DBR diode laser, the Yb amplifier and the PPLN crystal Peltier element, compact OEM diode laser current, and thermoelectric (TE) drivers were used. A TTL triggered relay controlled a beam shutter placed in front of the ECDL to allow a measurement of the detector dark voltage required for absolute transmission measurements. The data acquisition system used is similar to the one described in [4] and consisted of the output of the MCT detector preamplifier interfaced via a PCMCIA 16-bit A-D card to a notebook computer. Detector voltage was sampled at a rate of 100 kHz with a 9-kHz low pass filter (software implemented Gaussian filter). The data acquisition and analysis were controlled by Labview programming language.

The sensor, including all electronics, was placed on a 45×45 cm^2 optical breadboard, with an overall height of 12 cm. The weight was 25 kg and the entire sensor was then mounted in a reinforced plastic suitcase for portability. Power was supplied by 4×5 V, 2-A linear power supplies, and $2x \pm 15$ V, 200-mA linear power supplies. The ECDL used its commercial power supply and driver. Total power consumption is ~60 W.

To provide a continuous gas flow through the spectroscopic cell at a regulated pressure, a two-stage diaphragm pump was used in series with a pressure flow controller (MKS-640). A miniature Baratron pressure transducer (MKS-722) was used to measure the gas pressure just prior to the multipass cell. To reduce the interaction between the gas handling components and the gas mixtures, stainless steel or teflon tubing was used throughout the gas delivery system. Furthermore, for measurement of reactive gases (such as H_2CO, HCl, and NO_2) the gas handling system was maintained at ~40°C by use of heating tape. For the measurement of HCl, which reacts strongly with water and is in addition strongly polar, the gas system was purged for several hours by the use of high purity N_2 (H_2O concentration specified to be < 5 ppm).

3. EXPERIMENTAL RESULTS

The mid-infrared DFG power as a function of wavelength is shown in Fig. 3. The right-hand axis is the ECDL power (pump) available at the entrance facet of the PPLN. The 1083-nm power (signal) is kept constant at 540 mW. For incident powers of 6.2 and 540 mW of the pump and signal beams respectively, a maximum idler power of 2.8 µW at 3.46 µm was generated (cor-

rected for losses of 3.4% from the CaF$_2$ lens and a 4% wavelength-dependent loss of the Ge filter). The ECDL power delivered by the fiber peaks at 8.5 mW near 850 nm, corresponding to the gain center of the ECDL. The peak DFG conversion efficiency measured was 0.88 mW/W^2 for the 19-mm-long crystal at 3.3 μm. In comparison, the theoretical DFG conversion efficiency yields 1.69 mW/W^2 [11]. Factors that contribute to the reduced experimental conversion efficiency include nonmatching pump-beam mode field diameters in the fiber (1/e^2 diameters: 850 nm ~ 5.5 μm, 1083 nm ~ 6.6 μm) leading to incomplete overlap of the imaged pump beams in the crystal. The low NA (0.25) of the imaging lens will introduce spherical aberration into the focused beam spots. Some nonuniformity in conversion efficiency across individual PPLN channels has also been observed.

The measured PPLN phasematching and theoretically predicted phasematching are shown in Fig. 4 (using the Sellmeier coefficients published by Jundt [12]). For tuning the idler from 3.27- to 3.65-μm (Fig. 4a), the PPLN crystal was translated perpendicular to the optical axis across the 22.4- to 23.1-μm QPM channels (0.1-μm steps) at a constant temperature of 25°C. DFG wavelengths of 3.65–4.4 μm were phasematched using the 23.1-μm QPM channel and crystal temperatures from 25 to 110°C (shown in Fig. 4b). Agreement between theory and experiments is good, verifying that the Sellmeier coefficients for PPLN are accurate out to at least 4.4 μm. This result indicates that any wavelength in the mid-infrared tuning range of the DFG gas sensor can be conveniently accessed using a combination of crystal temperature and grating period. If a PPLN crystal with grating periods of 22.4–23.3 μm in 0.1-μm steps is used, the entire tuning range of the sensor can be conveniently phasematched using different grating periods and temperatures from 11 to 43°C.

The linewidth of the DFG sensor was measured indirectly by acquisition of a low-pressure Doppler-broadened line spectrum. In Fig. 5 a portion of a Doppler-broadened (0.4 torr) CH$_4$ spectrum near 3.3 μm in a 3-cm-length cell is shown. This spectrum was acquired at a sweep frequency of 100 Hz, and is an average of 100 scans. By fitting Gaussian absorption peaks to the individual absorption features, and then deconvolving the width with the calculated molecular Doppler width, 60 MHz was determined for the DFG linewidth (assumed to be Gaussian).

Direct absorption spectra of six species of interest for trace gas detection that are within the 3.25- to 4.4-μm tuning range of the sensor, including (a) CO$_2$, (b) N$_2$O, (c) H$_2$CO, (d) HCl, (e) NO$_2$, and (f) CH$_4$, have been acquired. These spectra have been obtained at reduced pressure (88 Torr) in a multipass cell with an effective path length of 18 m using either calibrated gas mixtures or room air. The integrated line-shape area was used to determine the molecular concentrations.
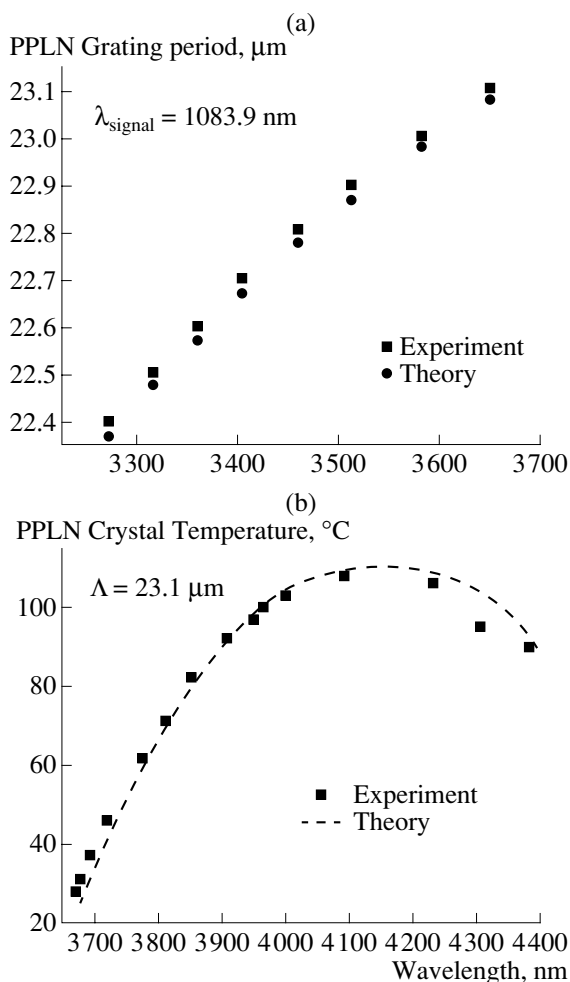

Fig. 4. Two quasi-phasematching approaches by changing nominal grating period (LHS) or temperature tuning at a fixed nominal grating period (RHS).

The peak-to-peak baseline noise evident from the recorded spectra is ± 0.02%, and is due to etalon effects in the optical path of the modulated pump beam. To acquire individual spectra, the DFG-based gas sensor was wavelength tuned by manually adjusting the ECDL wavelength (with reference to a wavemeter) and the phasematching conditions of the PPLN crystal were adjusted by a combination of translations to different QPM periods and temperature changes. No additional realignment of the sensor was required when the wavelength was changed, indicating that complete automation of sensor tuning should be straightforward using, say, a stepper motor. To remove baseline irregularities caused by etalons in the beam paths, a third-order polynomial was simultaneously fitted with a pressure-broadened Lorentzian lineshape using a nonlinear least squares algorithm (Levenberg–Marquardt). The data processing and fitting was accomplished in near-real-time (<2 s). For each spectrum the signal was averaged over the specified time, and subsequently the detector

Absorbance

0.4 torr CH_4, 3 cm pathlength
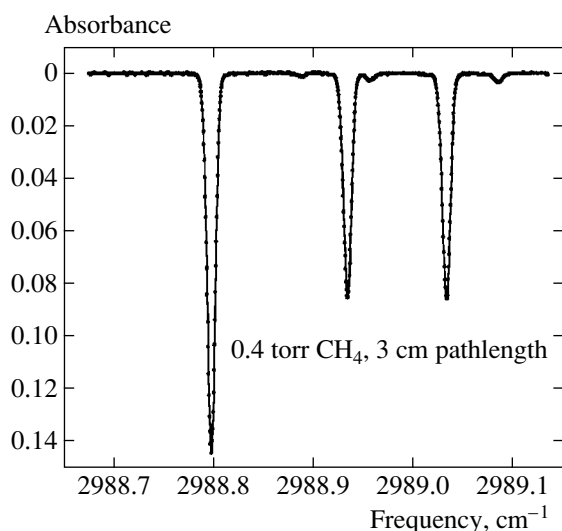
Fig. 5. Doppler-broadened 0.4 torr CH_4 [P(3)] spectrum near 3.3 μm. By fitting Gaussian absorption peaks to the individual absorptions features and deconvolving the peak width with the calculated molecular Doppler width, an estimate of <60 MHz was determined for the laser linewidth (assumed Gaussian).

dark voltage was measured (50 averages) to allow calculation of the absolute absorption.

In the table the data acquisition parameters are listed, and the measured spectral characteristics and concentrations are compared to the spectral data predicted from the Hitran96 database and the calibrated concentrations of the measured trace gases. In the case of HCl, the concentration was obtained from a calibrated cylinder specified at 24.4 ppm (in N_2), which we measured the HCl concentration to be 19.5 ± 0.2 ppm. This measurement alternatively used the $H^{35}Cl$ line at 2944.913 cm^{-1} and the $H^{37}Cl$ line at 2942.721 cm^{-1} ($S = 5.033 \times 10^{-19}$ cm/molecule and 1.606×10^{-19} cm/molecule, respectively). The minimum detectable concentration (MDC) value stated in the table was calculated for a single measurement and assumes $S/N = 1$ and an absorption measurement sensitivity of 4×10^{-4}.

The overall instrument performance, including repeatable precision and suitability of the sensor for long-term measurements, was assessed by monitoring of a discrete CH_4 line at 3038.751 cm^{-1} for an extended period of time. Experimental results obtained by continuous monitoring of ambient air for a 7-day period are shown in Fig. 6. This CH_4 concentration measurement used the Hitran96 predicted linestrength of 9.519×10^{-20} cm/molecule for the 3028.75 cm^{-1} line. The measurement standard deviation was $\pm 0.8\%$ (± 14 ppb), which corresponds to an absorption sensitivity of $\pm 2 \times 10^{-4}$.

4. DISCUSSION AND CONCLUSION

The use of fiber delivery and a WDM for beam combination has significantly improved the robustness and wavelength tuning capability of the sensor. During routine operation, the DFG power level was found to be stable over multiday operation.

To ensure stable sensor operation, care needed to be taken in packaging of the optical fibers, as any movement of pressure on the optical fibers affects the polarization of the pump beams and hence decreases the DFG conversion efficiency. Furthermore, the alignment was maintained (indicated by a constant DFG power level) when the sensor was relocated to an outside environment. These results are in contrast to our experience with the operation of DFG sensors based on discrete optics that required periodic minor realignments because of mirror and lens mount relaxation [3, 4]. In addition, by utilizing an efficient high-power Yb doped fiber amplifier we have eliminated the need for a high-power narrow linewidth source. This has been replaced with the requirement for a low-power (~several mW) amplifier seed source that can operate anywhere within the broad gain bandwidth of the Yb fiber amplifier (1020–1120 nm).

We have acquired spectra of six common trace gas species to demonstrate the versatility of this diode laser-based DFG sensor. The specific spectral lines we used for the detection of each molecule were chosen on the basis of the expected concentrations present and known interfering species. However, because of the extended continuous tuning range of this sensor, alternate absorption lines could be chosen for detection of low/high gas concentrations or in the presence of interfering molecule absorptions.

From this work, it was deduced that the current detection sensitivity is limited by the occurrence of etalons in the baseline, presently corresponding to absorbances of $\pm 2 \times 10^{-4}$. To compensate for these etalons and increase the absolute sensitivity of the absorption measurement, the use of a balanced detection scheme [14, 15] is expected to increase the routine detection limit to ~5×10^{-5}. This will involve a wedged beam sampling mirror placed prior to the multipass cell, which directs a small amount of the beam to a second detector, thereby allowing the nonlinear baseline to be normalized using the sampled baseline. This technique will not remove the fringes that originate from the multiple mirror reflections in the multipass cell, but it is possible to use a digital notch filter to reduce these etalon fringes. For extended operation the frequency drift of the diode lasers must be controlled; this is particularly pronounced until the sensor suitcase reaches a steady state temperature. Such active temperature control of the DBR diode laser requires a frequency reference based on an appropriate spectral feature acquired from a reference gas cell (which is periodically inserted into the beam path). Furthermore, a PPLN crystal with a "fan-out" QPM grating design [16] will replace the
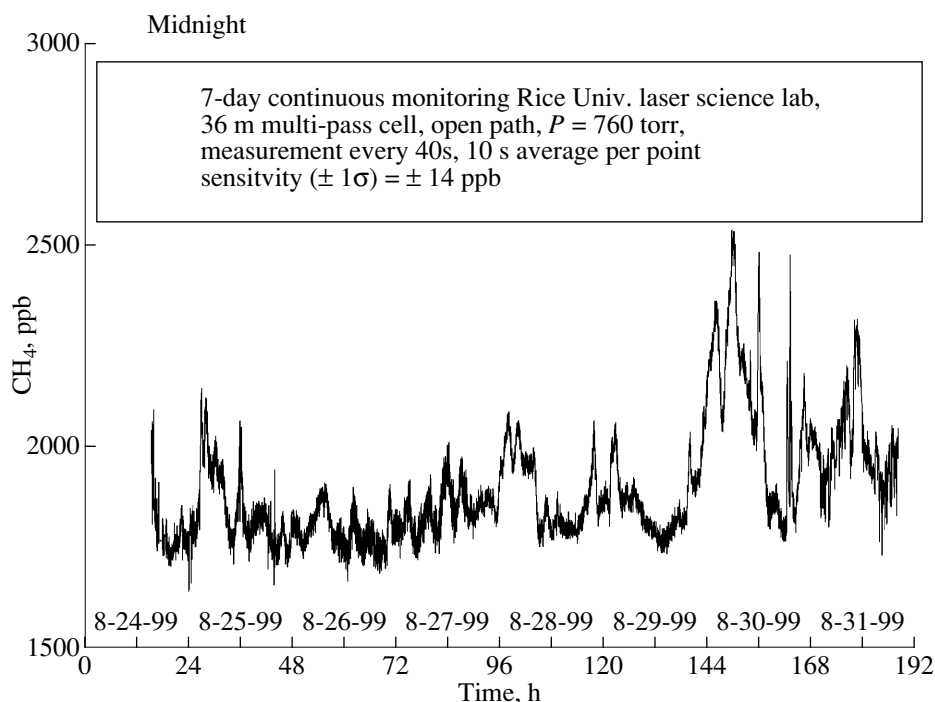
Fig. 6. Methane concentration measurements in ambient air 3028.8 cm^{-1} over a 7-day period.

discrete channel PPLN crystal, which will permit continuous DFG scans to be conducted by synchronously tuning one of the pump wavelengths while translating the crystal. DFG power scaling using watt-level in-line fiber amplifiers [17] is expected to increase the available mid-IR DFG power by a factor of 10–100, thereby improving the detector signal-to-noise, or allowing the use of IR detectors operating at room temperature without the need of Peltier cooling.

In conclusion, we have demonstrated a narrow-bandwidth DFG sensor with a 3.25- to 4.30-μm tuning range and generating up to 3 μW in the spectroscopically important 3- to 5-μm "fingerprint" region. By fiber coupling the pump sources and using a fiber coupler for combining the pump beams, routine alignment tasks have been eliminated. We have demonstrated sensitive, selective, and real-time detection of CH_4 at 3.3 μm by monitoring CH_4 in ambient air near 3028.8 cm^{-1} over a 7-day period. The measured standard deviation error corresponds to an absorption sensitivity of $\pm 2 \times 10^{-4}$. Furthermore, we have demonstrated the versatility of this sensor by recording spectra of six trace gas species: CO_2 (4.19 μm), N_2O (3.89 μm), H_2CO (3.53 μm), HCl (3.52 μm), NO_2 (3.47 μm), and CH_4 (3.30 μm). It will be possible to use the same device architecture in the future to extend the current spectral regime to longer wavelengths (5–16 μm) by using quasi-phase-matched GaAs when this material becomes available [18, 19].

Data acquisition parameters, measured spectral characteristics, and concentrations compared to the spectral data predicted by the Hitran96 database and the calibrated concentrations of 6 measured trace gas species

Gas species	Scan range (cm^{-1})	Averaging time (s)	Pressure (Torr)	Scan center cm^{-1} (μm)	Meas. conc.	Specified concentration	MDC (L = 18 m)
CO_2	0.34	2.1	88	2387.2(4.19)	444 ppm	room air	460 ppb
N_2O	0.29	2.1	88	2572.1(3.89)	315 ppb	room air	95 ppb
H_2CO	0.27	2.1	88	2831.7(3.53)	860 ppb	862 ± 15 ppb	54 ppb
HCl	0.33	2.1	87	2843.6(3.52)	19.5 ppm	24.4 ppm (±5%)	9 ppb
NO_2	0.28	2.1	88	2881.8(3.47)	7634 ppb	13.0 ppm (±5%)	259 ppb
CH_4	0.32	2.1	88	3028.7(3.30)	1756 ppb	room air	23 ppb

REFERENCES

1. Petrov, K.P., Curl, R.F., Tittel, F.K., *et al.*, 1996, *Opt. Lett.*, **21**, 86.

2. Töpfer, T., Curl, R.F., Tittel, F.K., *et al.*, 1997, *Appl. Opt.*, **36**, 8042.

3. Richter, D., Lancaster, D.G., and Tittel, F.K., 1998, *Appl. Phys. B*, **67**, 347.

4. Lancaster, D.G., Curl, R.F., and Tittel, F.K., 1998, *Appl. Phys. B*, **67**, 339.

5. Petrov, K.P., Curl, R.F., and Tittel, F.K., 1998, *Appl. Phys. B*, **66**, 531.

6. Seiter, M., Keller, D., and Sigrist, M.W., 1998, *Appl. Phys. B*, **67**, 351.

7. Goldberg, L., Lancaster, D.G., and Tittel, F.K., 1998, *Opt. Lett.*, **23**, 1517.

8. Lancaster, D.G., Goldberg, L., and Tittel, F.K., 1998, *Electron. Lett.*, **34**, 1345.

9. Goldberg, L., Moeller, R.P., and Kliner, D.A.V., 1998, *Opt. Lett.*, **23**, 1037.

10. Goldberg, L., Cole, B., and Snitzer, E., 1997, *Electron. Lett.*, **33**, 2127.

11. Canarelli, P., Benko, Z., Curl, R.F., and Tittel, F.K., 1992, *J. Opt. Soc. Am. B*, **9**, 197.

12. Jundt, D.H., 1997, *Opt. Lett.*, **22**, 1553.

13. Courtesy of Dlugokencky, E., NOAA, Climate Monitoring & Diagnostic Laboratory, Boulder CO.

14. Allen, M.G., Carleton, K.L., Davis, S.J., *et al.*, 1995, *Appl. Opt.*, **34**, 3240.

15. Lancaster, D.G., Richter, D., Curl, R.F., *et al.*, 1999, *Opt. Lett.*, **24**, 1744.

16. Powers, P.E., Kulp, T.J., and Bisson, S.E., 1998, *Opt. Lett.*, **23**, 159.

17. Goldberg, L., Koplow, J., and Kliner, D.A.V., 1999, *Opt. Lett.*, **24**, 673.

18. Zheng, D., Gordon, L.A., Wu, Y.S., *et al.*, 1998, *Opt. Lett.*, **23**, 1010.

19. Eyres, L.A., Ebert, C.B., Harris, J.S., Jr., and Fejer, M.M., 1998, *CNOM Annual Report 1997–1998*, Stanford University.